Flood Mapping and Damage Assessment Using UN-SPIDER Recommended Practices in Google Earth Engine: A Case Study of the 2024 Chiang Rai Flood, Thailand

Thammaboribal, P.,[1*] Tripathi, N. K.,[1] Lipiloet, S.[2] and Mandadi, R.[1]
[1]Asian Institute of Technology, School of Engineering and Technology, P.O.Box 4, Klong Luang, Pathumthani 12120, Thailand, E-mail: prapasgnss@gmail.com
[2]Department of Civil Engineering, Faculty of Engineering, Rajamangala University of Technology Thanyaburi, Pathumthani 12120, Thailand
**Corresponding Author*

DOI: https://doi.org/10.52939/ijg.v21i3.4039

Abstract
The 2024 Chiang Rai flood in Thailand highlighted the increasing frequency and severity of flood events driven by climate change and urbanization. This study applied the United Nations Platform for Space-based Information for Disaster Management and Emergency Response (UN-SPIDER) recommended practices to map flood extents and assess damages using Synthetic Aperture Radar (SAR) data from Sentinel-1 satellites in Google Earth Engine (GEE). The methodology involved change detection between pre-flood (1–9 September 2024) and post-flood (11–20 September 2024) SAR imagery, utilizing VH polarization for enhanced sensitivity to surface water. A threshold value of 1.25, recommended by UN-SPIDER, was identified as optimal through validation with ground data from the Geo-Informatics and Space Technology Development Agency (GISTDA), achieving 93.38% accuracy. The results indicated a total flood-affected area of 36,409 hectares, primarily along the Nam Kham, Nam Kok, and Nam Mae Ing rivers, with severe impacts in Mae Sai district. The study estimated 3,246 exposed individuals, 11,107 hectares of affected cropland, and 1,944 hectares of inundated urban areas. However, discrepancies arose when compared to GISTDA reports, particularly in cropland and population estimates, due to differences in data resolution and methodologies. The UN-SPIDER approach demonstrated scalability and efficiency for near-real-time flood monitoring, though limitations included challenges in urban flood detection and reliance on Sentinel-1's acquisition frequency. The findings underscore the utility of satellite-based flood mapping for disaster management while emphasizing the need for higher-resolution data to improve accuracy. This study contributes to flood risk mitigation strategies by providing actionable insights for policymakers and disaster response teams in Chiang Rai and similar flood-prone regions globally.

Keywords: Chiang Rai, Flood, Google Earth Engine, SAR, Sentinel 1, UN-SPIDER

1. Introduction

Flooding is one of the most widespread and devastating natural disasters, with far-reaching consequences for communities, economies, and ecosystems across the globe [1]. According to the United Nations, floods have become more frequent and severe in recent years, exacerbated by factors such as climate change, rapid urbanization, and the increasing frequency of extreme weather events [2]. Globally, floods account for significant loss of life, infrastructure damage, displacement, and long-term economic setbacks [3], particularly in low-lying areas and regions vulnerable to heavy rainfall, snowmelt, or coastal storm surges. In the face of these growing challenges, timely and accurate flood monitoring, coupled with effective damage assessment, is essential to mitigate the impact of such disasters and guide the recovery process [4] and [5].

Remote sensing technologies, particularly satellite imagery, have emerged as powerful tools for flood detection and monitoring [6]. Among the available options, the European Space Agency's Sentinel-1 satellites, equipped with Synthetic Aperture Radar (SAR), offer a reliable and efficient means of assessing flood extents [7].

Unlike optical imagery, SAR data can penetrate cloud cover and work in all weather conditions, making it particularly useful for real-time flood monitoring [8]. The United Nations Platform for Space-based Information for Disaster Management and Emergency Response (UN-SPIDER) has been at the forefront of promoting the use of satellite data for disaster response, providing guidelines and recommended practices for the effective use of satellite-based information in disaster management [9]. Among these practices, UN-SPIDER has outlined a framework for using Sentinel-1 data to detect flooded areas, assess the severity of the flood event, and evaluate the resulting damage [10].

This study focuses on the application of UN-SPIDER's recommended practices for flood mapping and damage assessment in the context of the September 2024 flooding in Chiang Rai province, Thailand. Located in the northern region of Thailand, Chiang Rai shares a border with Myanmar and is prone to seasonal flooding due to the monsoon rains that typically occur between May and October. The province's agricultural sector, vital infrastructure, and transportation routes are all vulnerable to flooding during the rainy season. Additionally, the geographical location of Chiang Rai, straddling the border between Thailand and Myanmar, makes it a critical economic zone, with cross-border trade routes, markets, and supply chains heavily impacted by flood events.

In September 2024, Chiang Rai experienced one of the most severe floods in recent years. The flood was triggered by a combination of heavy rainfall from the monsoon season, overflowing rivers, and inadequate drainage systems in some areas. The floodwaters inundated large swathes of land, including agricultural fields, residential areas, and key infrastructure. The affected region not only faced significant damage to crops and property but also witnessed disruptions in trade between Thailand and Myanmar, as essential roads and bridges were submerged, halting transportation and economic activities [11]. Flooding in Chiang Rai is a recurrent problem, especially during the monsoon months. The floods are typically caused by a combination of factors, including heavy rains, rapid snowmelt from the mountainous regions of the Himalayas, and the overflow of the Kok River and its tributaries. These floods often result in damage to agricultural lands, the destruction of infrastructure such as roads and bridges, and disruptions to local economies and communities. In addition to the direct physical damage, seasonal floods in Chiang Rai also cause longer-term impacts, including soil erosion, water contamination, and loss of livelihoods, particularly for those dependent on agriculture [12].

In recent years, the frequency and intensity of flooding in Chiang Rai have increased due to the combined effects of climate change and urbanization. The impacts of more erratic weather patterns, such as heavier rainfall over shorter periods and more intense storms, have made the region even more vulnerable to flooding. The September 2024 flood, which is the focus of this study, serves as a stark reminder of the destructive power of flooding in Chiang Rai. The flood was triggered by exceptionally heavy rainfall during the monsoon, causing rivers to exceed their capacity and inundating large areas of the province, especially those near the Kok River.

In addition to the local impacts of flooding, Chiang Rai's proximity to Myanmar adds an extra layer of complexity to flood events. The province is a critical hub for cross-border trade and transportation, linking Thailand with Myanmar and, by extension, the broader Southeast Asian region. Flooding in Chiang Rai disrupts not only local communities and businesses but also transnational trade routes, which can exacerbate economic losses in both Thailand and Myanmar. This makes effective flood monitoring and damage assessment even more crucial, as it is essential to understand both the local and cross-border implications of such disasters.

The primary objective of this study is to apply the UN-SPIDER recommended practices [10] to map the flooded areas in Chiang Rai and assess the resulting damages. By leveraging Sentinel-1 data in Google Earth Engine, this research seeks to provide accurate and timely flood mapping, identifying the extent and severity of the flooding across the province. Additionally, the study will evaluate the damage to critical infrastructure, agricultural land, and residential areas, providing valuable insights into the socioeconomic impact of the flood. The information generated by this study will be useful for local authorities, disaster management teams, and policymakers, assisting them in making informed decisions for response, recovery, and future flood risk management.

2. Methodology

2.1 Study Area

Chiang Rai is located in the northernmost region of Thailand, bordered by Myanmar to the north and Laos to the east. This strategic position places Chiang Rai at the convergence of several important river systems, including the Mekong River to the east and the Kok River, which flows through the province (Figure 1).

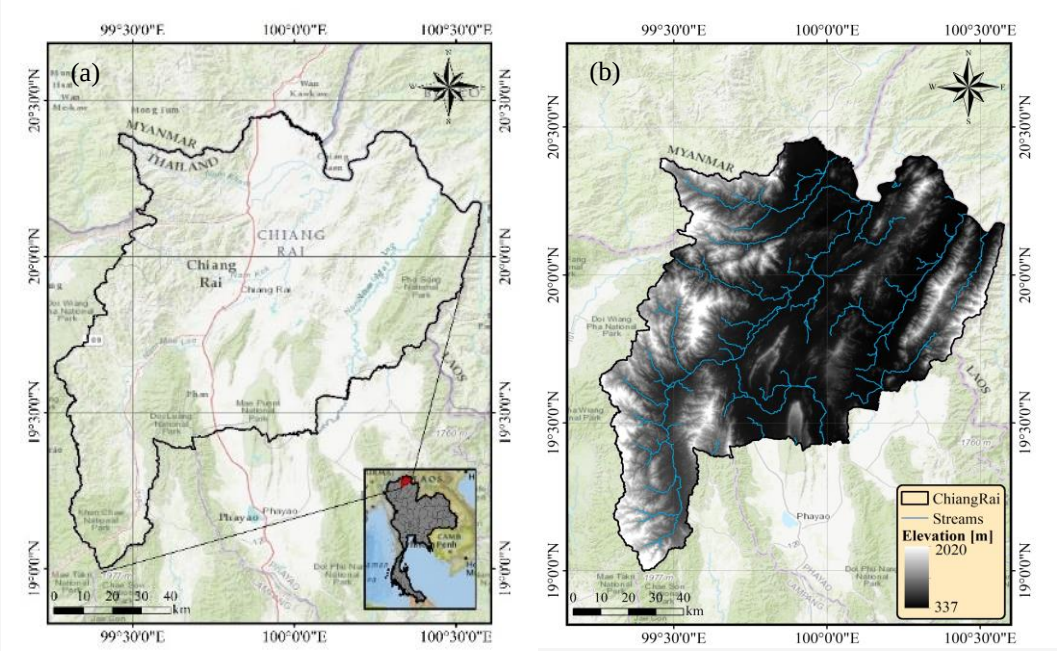

Figure 1: (b) Chiang Rai province of Thailand (b) DEM

The province is characterized by a mix of mountainous terrain in the north and lowland plains in the south, with elevations ranging from lowlands at approximately 200 meters to the peaks of the Himalayan foothills, which rise above 2,500 meters. This varied topography contributes to the region's vulnerability to flooding, particularly in areas near rivers and lower elevation zones. The province of Chiang Rai experiences a tropical climate influenced by the Southwest Monsoon, which brings heavy rainfall from May to October each year. During this monsoon season, rainfall is concentrated, often resulting in large-scale precipitation events that significantly impact the region's hydrological systems. On average, Chiang Rai receives between 1,500 and 2,000 millimeters of rainfall annually, with the highest rainfall typically occurring between August and September. This period corresponds with the peak of the monsoon, when moisture-laden winds from the Indian Ocean bring persistent rainfall across the region. The heavy rainfalls during this time contribute to rising river levels and saturated soil conditions, setting the stage for frequent flooding events. Chiang Rai is particularly susceptible to flooding due to its location within several river basins. The Kok River, which flows from the north and meanders through the province, is a major source of flooding when it overflows its banks, particularly during periods of intense rainfall. In addition to riverine flooding, Chiang Rai's geography and terrain exacerbate flood risks, as the province includes both urban and rural areas situated in flood-prone lowland zones. These low-lying areas are more vulnerable to the accumulation of floodwaters, especially when drainage systems are overwhelmed or insufficient to manage the volume of water.

Given the geography, seasonal rainfall patterns, and recurrent flood events in Chiang Rai, this province represents an ideal study area for applying advanced satellite-based flood mapping techniques. By using Sentinel-1 data in Google Earth Engine and adhering to UN-SPIDER's recommended practices, this study aims to provide a detailed analysis of flood occurrence, map flooded areas accurately, and assess the resulting damage. The findings from this study will help improve flood risk management and contribute to disaster preparedness strategies, not only for Chiang Rai but also for similar flood-prone regions around the world.

2.2 UN-SPIDER

The United Nations Platform for Space-based Information for Disaster Management and Emergency Response (UN-SPIDER) is an initiative established by the United Nations Office for Outer Space Affairs (UNOOSA). Its primary goal is to enhance the use of space-based technologies, particularly satellite data, in disaster management, emergency response, and risk reduction. UN-SPIDER provides a global platform for sharing knowledge and expertise, fostering collaboration between space agencies, governments, humanitarian organizations, and disaster management professionals.

The platform aims to bridge the gap between space technologies and disaster management practitioners by promoting the integration of satellite-based information in disaster preparedness, response, and recovery efforts. One of the key aspects of UN-SPIDER's work is the development of guidelines and recommended practices for using space-based data in disaster management. For flood mapping and damage assessment, UN-SPIDER offers specific recommendations for using Earth observation data, particularly from satellites like Sentinel-1, which is equipped with Synthetic Aperture Radar (SAR). These guidelines focus on utilizing satellite imagery to accurately detect flooded areas, assess the extent of the flood, and evaluate the resulting damage to infrastructure, agriculture, and communities.

UN-SPIDER recommends the use of radar-based sensors, such as those on the Sentinel-1 satellites, for flood mapping due to their ability to capture data in all weather conditions, including during heavy rainfall or cloud cover. The SAR data from Sentinel-1 is especially effective for detecting changes in the Earth's surface caused by floods, as the radar waves can differentiate between flooded and non-flooded areas based on the presence of standing water. The recommended process involves the use of pre- and post-event satellite images to identify the extent of the flood and its impacts on both urban and rural areas. For damage assessment, UN-SPIDER suggests combining satellite-based flood maps with other sources of information, such as ground-level observations and data from other satellite systems. This multi-source approach helps to more accurately quantify the damage to infrastructure, agricultural fields, and other vital resources. The goal is to provide disaster managers with a clear understanding of the scale of the disaster, allowing for more effective response planning, resource allocation, and recovery efforts. By following these recommended practices, disaster management agencies can make more informed decisions, ultimately leading to faster recovery and better preparedness for future flood events. The guideline of UN-SPIDER recommendation that adopted in this study is available at [10].

2.3 Sentinel -1 Satellite Imagery

The Sentinel-1 satellite constellation, part of the European Space Agency's (ESA) Copernicus program, provides invaluable data for flood mapping and monitoring. Sentinel-1 consists of two satellites, Sentinel-1A and Sentinel-1B, which are equipped with Synthetic Aperture Radar (SAR) [13]. The SAR imagery can be acquired from https://browser.dataspace.copernicus.eu/. Unlike optical satellites, SAR can capture data in all weather conditions, including through clouds and at night, making it particularly well-suited for flood monitoring, especially in regions prone to heavy rainfall or frequent cloud cover. Sentinel-1 provides frequent revisits (every 6 to 12 days, depending on location), ensuring timely monitoring of flood events and their progression. This is especially important for real-time flood detection and post-flood damage assessment [14]. Sentinel-1's ability to capture pre-flood and post-flood images makes it a powerful tool for assessing the extent and severity of flood events (Figure 2). By comparing satellite images taken before and after a flood event, the areas impacted by flooding can be easily identified [15] and [16].

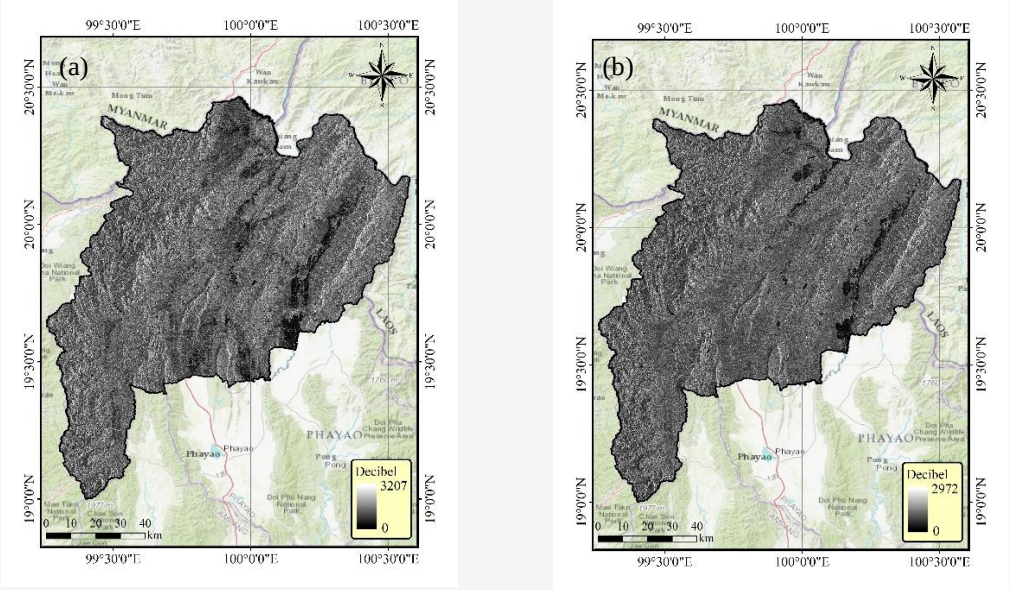

Figure 2: Sentinel-1 SAR imagery: (a) pre-flood (b) post-flood

Changes in the radar signal due to the presence of standing water or altered surface conditions provide clear indicators of flood extent, enabling the creation of accurate flood maps.

2.4 Google Earth Engine

Google Earth Engine (GEE) is a cloud-based platform that provides access to an extensive archive of geospatial data, including satellite imagery, environmental data, and topographic maps. It is widely used for various environmental monitoring and analysis tasks, including flood mapping [17][18] and [19]. The platform leverages powerful computational resources and advanced geospatial algorithms, making it ideal for processing large volumes of satellite data efficiently. For flood mapping, Google Earth Engine allows users to access and analyze high-resolution satellite imagery, such as that from Sentinel-1, Landsat, and other Earth observation satellites, enabling rapid detection and assessment of flood events. One of the key advantages of using Google Earth Engine for flood mapping is its ability to manage and process vast amounts of satellite data. Google Earth Engine integrates multiple data sources and offers tools for time-series analysis, allowing users to easily compare pre- and post-flood imagery to detect changes in the landscape caused by flooding. For instance, Sentinel-1 radar data, available through GEE, can be used to identify flood extent by detecting areas where water has accumulated and analyzing the changes in surface reflectance. GEE's processing capabilities allow for quick identification of flood-affected regions, even in areas with dense cloud cover, which would otherwise be difficult to assess using optical imagery alone.

Another key feature of Google Earth Engine is its ability to perform automated image classification and change detection [20] and [21]. This is particularly useful in flood mapping, as it enables the automated identification of flooded areas from satellite imagery without manual interpretation. Using machine learning algorithms and spectral analysis, GEE can classify different land cover types and distinguish between areas of water and land, even in complex or rural environments. Additionally, time-series analysis allows for the monitoring of flood dynamics over time, enabling real-time tracking of flood events as they evolve. In addition to mapping flood extents, Google Earth Engine also enables damage assessment by integrating other spatial datasets, such as population density maps, infrastructure data, and land use information. This allows for a more comprehensive analysis of flood impacts, helping authorities to identify areas of high vulnerability, prioritize emergency response efforts, and assess the long-term effects on communities and infrastructure [22] and [23]. Overall, Google Earth Engine plays a pivotal role in modern flood mapping and disaster management. Its robust analytical tools, vast data repository, and cloud-based platform make it an indispensable tool for monitoring flood events, assessing damages, and informing decision-making processes in real-time [24].

3. Methodology

The flood extent is derived by performing change detection between pre-flood and post-flood Sentinel-1 SAR imagery, as illustrated in Figure 3.

1. Import the script copied from https://www.un-spider.org/sites/default/files/Code_GEE_flood_mapping.txt in GGE code editor.
2. Import the study area in shapefile format into the "Assets" tab of GEE. Ensure that the shapefile includes the .shp, .dbf, and .shx files for it to be opened successfully in GEE.
3. The timeframe for pre-flood and post-flood periods should be defined. The flood in the study area occurred on 11 September 2024. Therefore, the pre-flood period spanned from 1 to 9 September 2024, while the post-flood period covered 11 to 20 September 2024. The pre-flood and post-flood SAR imagery shown in Figure 4.
4. SAR imagery contains both VV and VH polarization [25], thus the selection of the polarization must be performed. Although VV and VH polarizations can be used for flood mapping [26], VH polarization is often considered more suitable due to its higher sensitivity to changes on the land surface and water reflection, making it better for delineating flooded areas [10].
5. To ensure accurate change detection, it is crucial to select the same pass direction for the images being compared, as variations in viewing angles could lead to false positive signals. Depending on the study area, the user can opt for either the “DESCENDING” or “ASCENDING” pass direction.
6. Run the script for change detection. The script implements a straightforward change detection method, where the post-flood mosaic is divided by the pre-flood mosaic to generate a raster layer that reflects the extent of change at each pixel.
7. A digital elevation model (WWF HydroSHEDS), derived from SRTM data with a spatial resolution of 3 arc-seconds, is used to exclude areas with slopes greater than 5%. Additionally, the connectivity of flood pixels is evaluated to remove those connected to eight or fewer neighboring pixels.

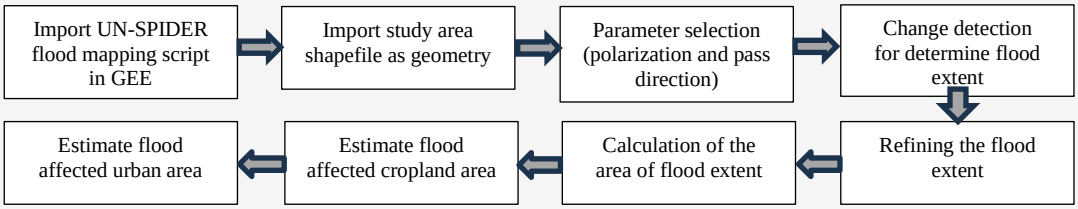

Figure 3: Flood extent extraction workflow

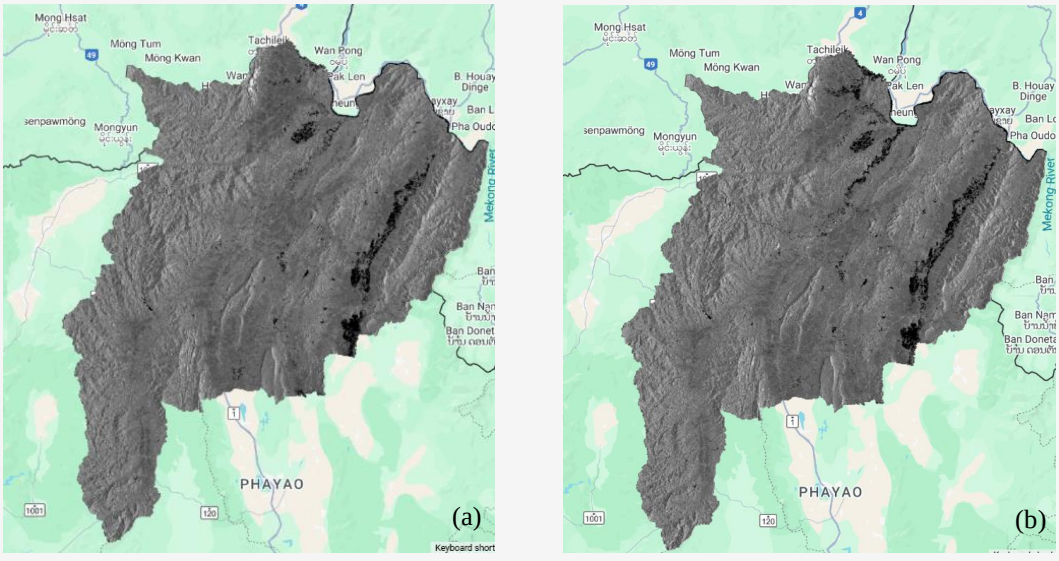

Figure 4: SAR imagery on Google Earth Engine (a) pre-flood (b) post flood

8. To calculate the flood extent area, a new raster layer is generated that computes the area in square meters for each pixel, considering the projection. By aggregating the values of all pixels, the total area is determined and then converted into ha. The final result is shown in the 'Results' panel located in the bottom-left corner of the Map Viewer.
9. To estimate the number of people affected by the flood, the code utilizes the JRC Global Human Settlement Population Layer (https://humansettlement.emergency.copernicus.eu/download.php?ds=pop), which has a 250 m resolution and was last updated in 2015 (Figure 5). This layer provides data on the population in each cell. In order to overlay the flood layer with the population data, the flood extent raster must first be reprojected to match the resolution and projection of the population dataset. Afterward, an intersection of both layers is performed, resulting in a new raster layer. The total number of exposed individuals is then calculated by summing the pixel values from the exposed population raster, with the final figure displayed in the 'Results' panel of the Map Viewer.
10. To estimate the extent of affected cropland, the MODIS Land Cover Type product was selected. This dataset, with a spatial resolution of 500 m, is updated annually and is currently the only global Land Cover dataset available in Google Earth Engine (Figure 6). The Land Cover Type 1 band includes 17 classes, two of which are related to cropland: class 12 (at least 60% of the area is cultivated) and class 14 (Cropland/Natural Vegetation Mosaics, representing small-scale cultivation with 40-60% cultivated area alongside natural tree, shrub, or herbaceous vegetation). Both of these classes are extracted and intersected with the flood extent layer, which has been resampled to match the scale and projection of the MODIS dataset.
11. The affected urban areas are determined in the same manner as the previous steps, using the MODIS Land Cover Type dataset. The "*Urban Class 13*" from the "*Land Cover Type 1*" band is extracted to identify potentially impacted urban regions. However, it is important to note that the estimation of affected urban areas may be underestimated, as detecting water in built-up areas can be challenging.

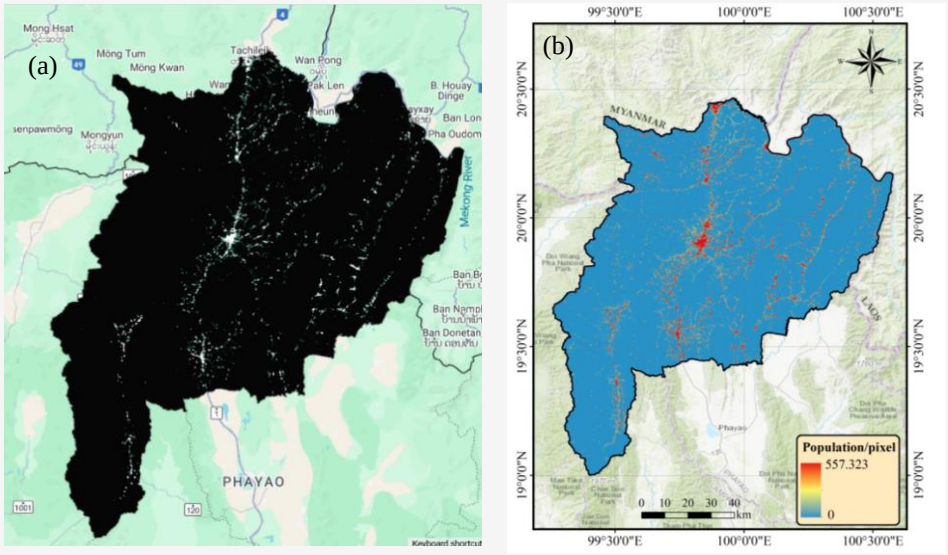

Figure 5: Global human settlement population illustration: (a) from script (b) form JRC

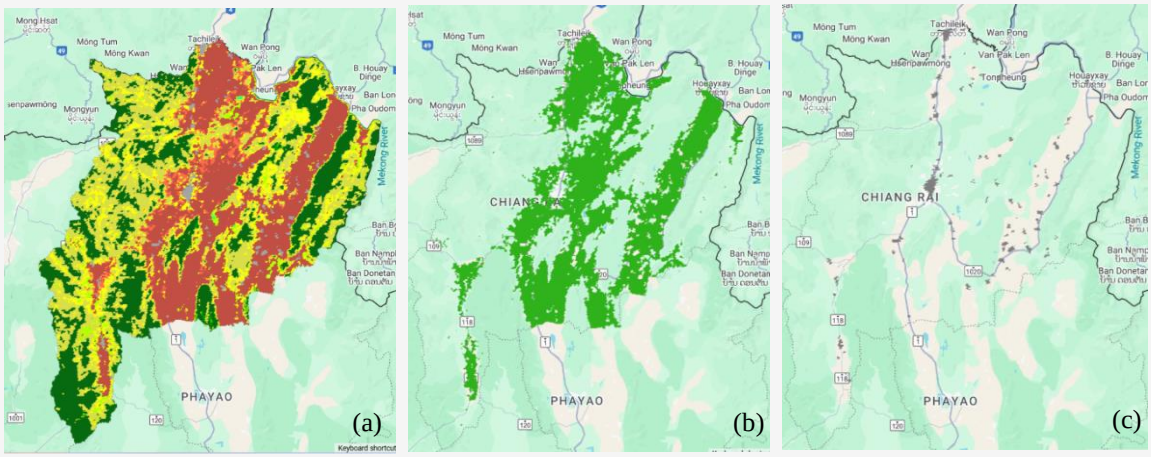

Figure 6: Land cover classification: (a) land cover (b) crop land (c) urban area

4. Results and Discussions

The results generated by the script provided by UN-SPIDER include the affected urban areas, impacted cropland, flooded regions, urban areas, cropland, land cover, exposed population, population density, and the SAR imagery difference between pre-flood and post-flood. Users can visualize their preferred results from the Layer tab, highlighted in a yellow rectangle. Additionally, the results showing the affected area, estimated number of exposed people, estimated affected cropland area, and estimated affected urban area are displayed in the blue rectangle in Figure 7.

4.1 Flood Extent Extraction

The flood extent was determined using a change detection method, defined as the ratio between post-flood and pre-flood SAR imagery. The change detection result depicts in Figure 8. Figure 8 shows that high values (lighter pixels) represent significant change, while low values (darker pixels) indicate minimal change. In order to extract the flooded area from the change map, a threshold must be assigned to separate the flooded and non flooded area. The optimum threshold value is not specified, it it must be determined through trial and error and can be adjusted if there are high rates of false positives or false negatives. In this study, the threshold varied from 1.10 to 1.40. Additionally, a threshold value of 1.25 was also applied, as it is the value recommended by UN-SPIDER. Once the threshold is specified, a value of 1 is assigned to values greater than the threshold, while a value of 0 is assigned to values below the threshold.

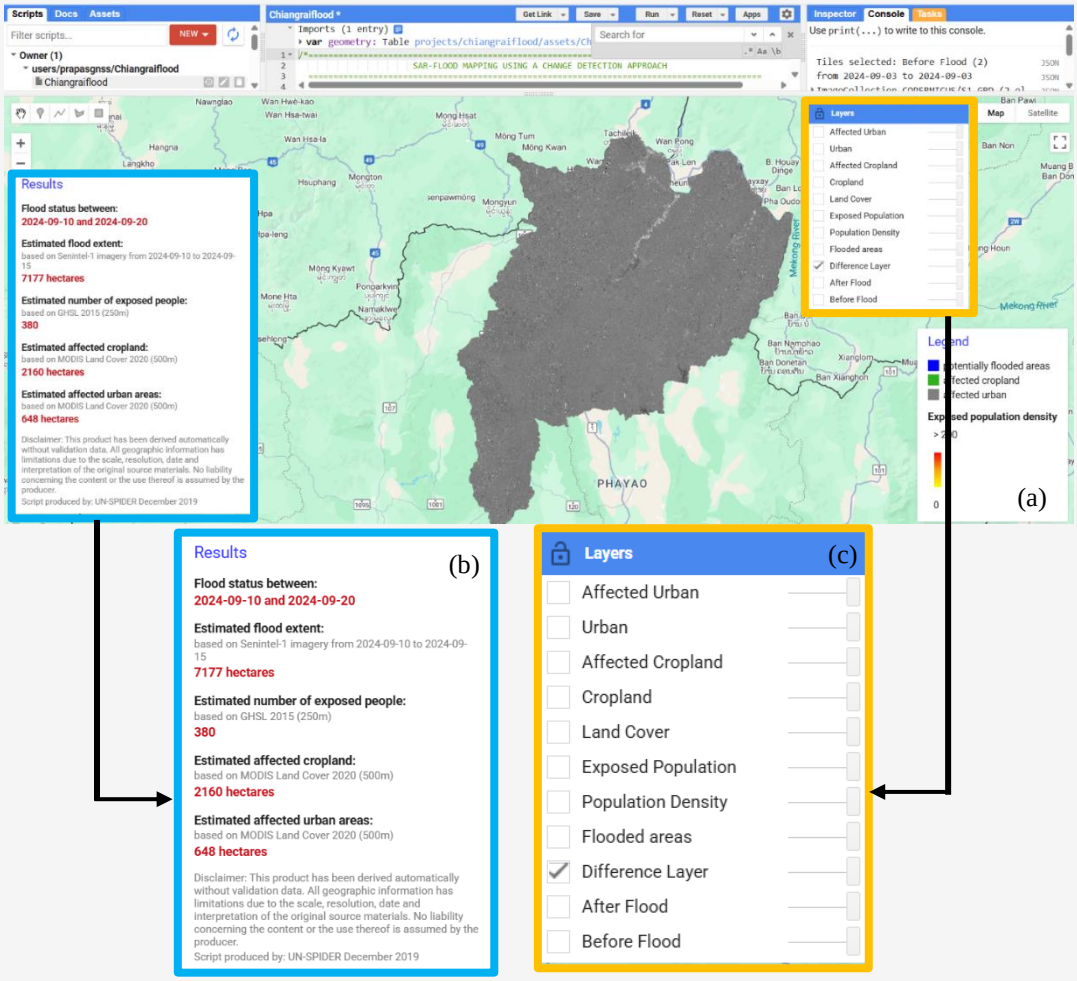

Figure 7: Result of the flood analysis:
(a) visualization of the results (b) flood affected areas (c) layer selection

Figure 8: Extent of change derived from pre- and post-flood SAR imagery

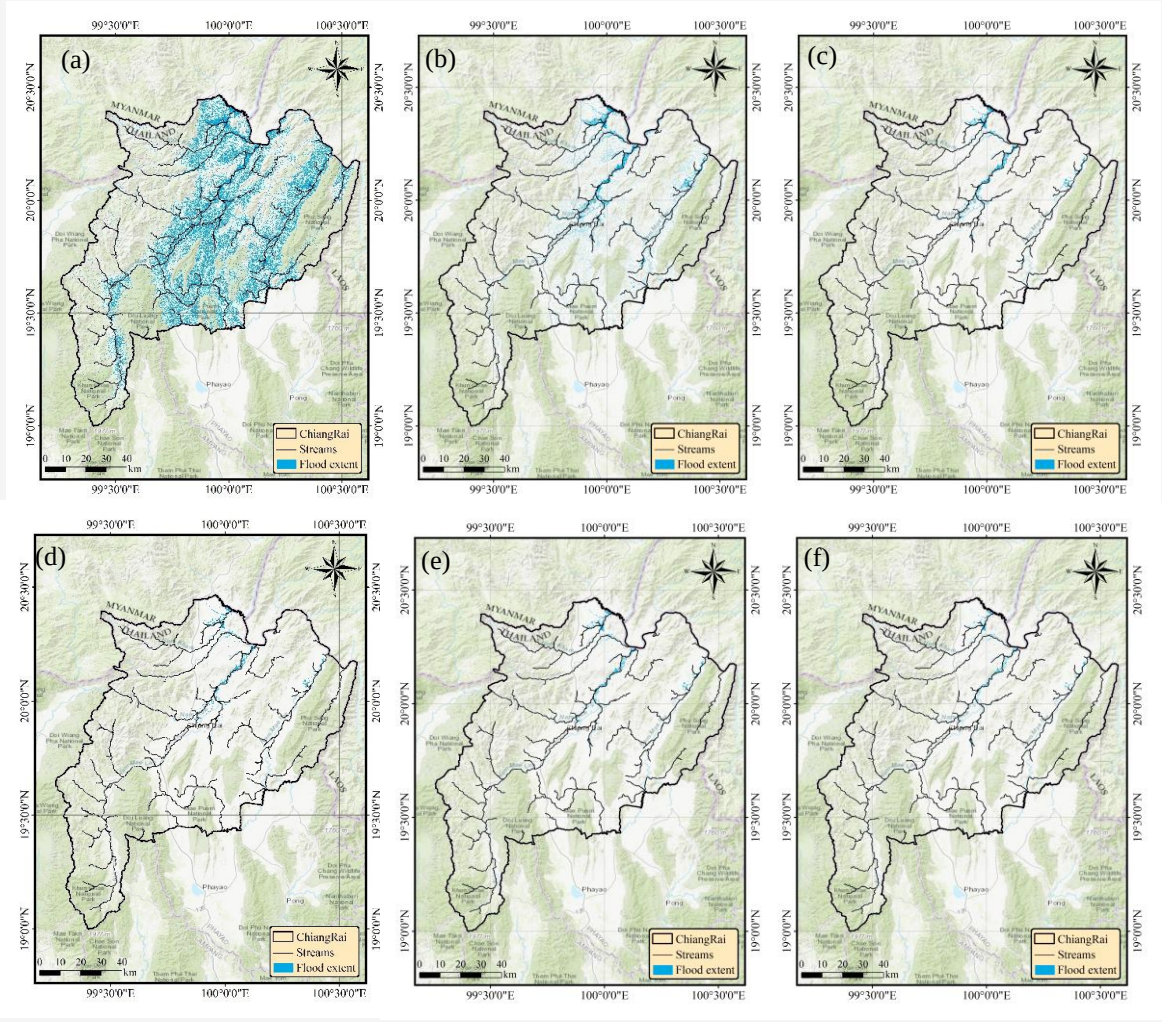

Figure 9: Flood extend derived from different threshold value:
(a) 1.00 (b) 1.10 (c) 1.20 (d) 1.25 (e) 1.30 (f) 1.40

The potential flood extent is then generated from the binary raster layer, highlighting the flooded areas. The results of the flood extent derived from different thresholds are shown in Figure 9. Figure 9 clearly demonstrates that the extent of the flooded area is strongly influenced by the threshold value used in flood delineation. As the threshold value decreases, the flooded area increases. Therefore, to determine the optimal value for the flood extent area, a trial-and-error approach must be employed, with validation of the results against the actual flooded area. Figure 7(a) shows that a threshold value of 1.00 results in the largest flooded area; however, this does not align with the actual flooded area in Chiang Rai province. For threshold values ranging from 1.10 to 1.40, the flooded areas are indistinguishable to the naked eye, indicating that further validation is necessary.

4.2 Validation of Flood Model

The confusion matrix was used for validating the flood model [27]. Actual flood data was obtained from https://www.gistda.or.th/. The flooded points, extracted from the flood-affected area map provided by the Geo-Informatics and Space Technology Development Agency (GISTDA), were utilized for the validation process. A total of 80 sampling points were used for validation. Although the results in Figure 9 show that the flood extent areas derived from threshold values between 1.20 and 1.40 do not differ significantly on the maps, validation with the actual flooded area from September 11, 2027, as shown in Table 1, revealed that the optimal threshold value is 1.25, with an accuracy of 93.38%. In contrast, a threshold value of 1.00 yielded the lowest accuracy of 60.50%.

Table 1: Confusion matrix for the selection of optimum flood threshold

Threshold	Class	Model Positive	Model Negative	Accuracy [%]
1.00	Actual Positive	60	20	60.50
	Actual Negative	52	28	
1.10	Actual Positive	65	15	76.88
	Actual Negative	22	58	
1.20	Actual Positive	72	8	85.63
	Actual Negative	15	65	
1.25	Actual Positive	76	4	93.38
	Actual Negative	5	75	
1.30	Actual Positive	75	5	91.25
	Actual Negative	9	71	
1.40	Actual Positive	73	7	88.13
	Actual Negative	12	68	

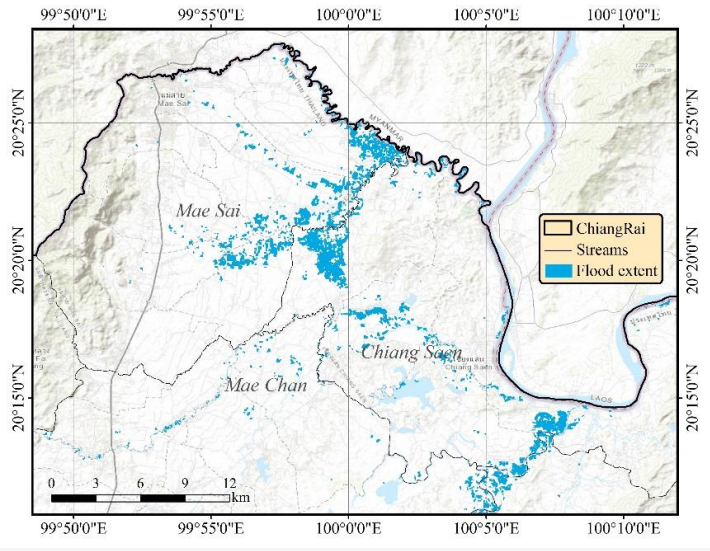

Figure 10: Most effected flooded areas in Mae Sai and Chiang Saen districts

As seen in Figure 9(a), flooded areas were observed across the entire study area; however, in reality, flooding only occurred in the northern part of the study area, specifically along the rivers in Mae Sai and Chiang San districts. The optimal threshold of 1.25 aligns with the value recommended by UN-SPIDER. Additionally, a threshold value of 1.30 is also acceptable, with an accuracy of 91.25%. Therefore, the flood extent map in Figure 9(d) was used to assess the affected area, focusing on both urban and agricultural zones. The expanded flood extent area, derived from the optimal threshold value of 1.25, is shown in Figure 10.

According to Figure 10, the affected flooded areas were primarily located along three main rivers: Nam Kham, Nam Kok, and Nam Mae Ing. The flooding was particularly concentrated in the northern part of Chiang Rai, with the Mae Sai district being especially affected. It's obviously seen that Mae Sai district was severely affected by flooding due to a combination of natural and human factors. The region experienced intense rainfall associated with the monsoon season, which typically occurs from May to October. This heavy rainfall led to river overflow, particularly along the Mae Sai River and its tributaries, causing widespread flooding in low-lying areas. The district's geography, characterized by mountainous terrain and steep slopes, contributed to rapid surface runoff during the heavy rains. The overflow from rivers, combined with reduced natural absorption due to deforestation and land use changes, exacerbated the flood situation. Additionally, inadequate infrastructure, such as drainage systems, may have been insufficient to handle the volume of water, further worsening the flooding. Lastly, the impacts of climate change, which can lead to more unpredictable weather patterns and heavier rainfall, may have also played a role in intensifying the flood event in Mae Sai. Together, these factors made the district particularly vulnerable to the severe flooding observed in September 2024.

4.3 Land Cover Classification

To estimate the flooded areas in urban and agricultural zones, land cover classification must be conducted. Typically, land use/land cover (LULC) classification is performed as an additional process using a supervised classification technique [28]. Landsat or Sentinel-2 satellite imagery are commonly used for this classification. However, in the script, land cover data from the MODIS Land Cover Type dataset of 2020 with spatial resolution of 500 m was utilized. The "Urban Class 13" of the band "Land Cover Type 1" is extracted to assess potentially affected urban areas. The land cover, urban areas, and crop land areas are illustrated in Figure 9. The land cover map is automatically displayed on the GEE screen, as shown in Figure 9(a). Subsequently, crop land and urban areas are automatically extracted from the land cover map, as illustrated in Figures 9(b) and 9(c). The flood extent area is then overlaid onto the urban and crop land areas to estimate the flood-affected areas for both land cover types.

4.4 Flooded Affected Area Assessment

The flood assessment includes the period of the flood, which matches the post-flood time span outlined in the script. The flood extent, affected cropland area, affected urban area, and the estimated number of exposed people were all automatically calculated. The results are shown in Figure 11. Using a threshold value of 1.25 for the period from September 10 to 20, 2024, the total flood-affected area for the entire Chiang Rai province was calculated to be 36,409 ha. The estimated number of people exposed to the flood was 3,246, determined from the 2015 Global Human Settlement Layer (GHSL) data with a spatial resolution of 250 m. The affected cropland and urban areas were estimated at 11,107 ha and 1,944 ha, respectively. The urban area impacted by the flood is highlighted within the red rectangle in Figure 11(b). The flood affected area and number of flood affected people was officially reported by GISTDA available at https://www.gistda.or.th/news_view.php?n_id=8084&lang=EN. The reports depicts in Figure 12. The total flooded area across the entire province was 233,908 rai, equivalent to 37,425.08 ha. The number of affected individuals was 47,888, and the area of damaged crops totaled 152,472 rai (24,395.52 ha). The difference in the flooded area calculated using the UN-SPIDER script and GISTDA data was 1,016 ha, which represents a 2.71% discrepancy.

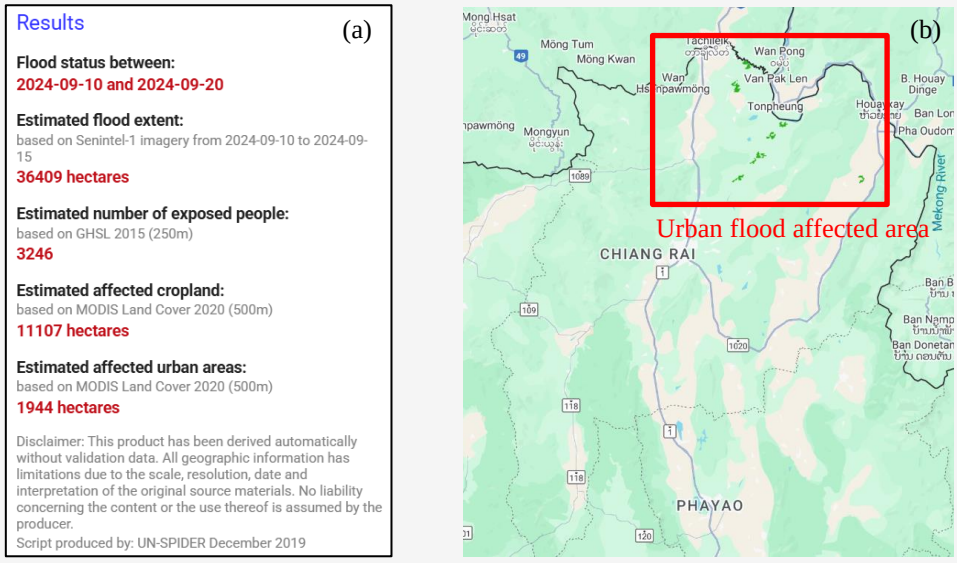

Figure 11: Assessment of flooded area (a) total results (b) urban flood affected area

Figure 12: Flood affected report of Chiang Rai on 16 September 2024

This result indicates that the UN-SPIDER recommendation, which uses a threshold value of 1.25 for flood extent extraction, aligns closely with the results reported by GISTDA. The primary cause of this difference is the discrepancy in the acquisition dates of the Sentinel-1 data. The UN-SPIDER data covered the period from September 10–20, 2024, while GISTDA used data from September 16, 2024. Despite this difference in data acquisition timing, the 2.71% variation is considered acceptable. Consequently, the UN-SPIDER recommended practices and the provided script are appropriate for identifying flood extent in the study area and can be generalized to other regions. Users can adjust the time span to capture flood events before and after the flood and modify the threshold to fine-tune the model, thereby enhancing its reliability for different study areas.

The difference in the affected cropland area between the UN-SPIDER script and GISTDA was 13,288 ha. This significant discrepancy was primarily due to the different satellite imagery used for land cover classification. The UN-SPIDER script relied on 2020 MODIS land cover data, which has a spatial resolution of 500 m, while GISTDA used different satellite imagery for land cover classification. As a result, a large error in the difference was observed. For example, one pixel of MODIS land cover corresponds to 250,000 sq.m., while pixels from Landsat and Sentinel-2 have spatial resolutions of 900 sq.m. and 100 sq.m., respectively. This difference in spatial resolution plays a crucial role in determining flood-affected areas. To improve the accuracy of identifying affected cropland or urban areas, land use/land cover (LULC) classification should be carried out using Landsat or Sentinel-2 imagery, which have higher spatial resolutions compared to MODIS. Therefore, the LULC used in the "Affected Agricultural Land" and "Affected Area" sections of the script should be replaced with LULC based on supervised classification using Landsat or Sentinel-2 data, instead of the MODIS land cover. In conclusion, the affected cropland area derived from the UN-SPIDER script may not provide an accurate representation of flood-affected areas in cropland. Furthermore, the accuracy of affected urban areas can be improved utilizing higher spatial resolution satellite imagery. The number of affected people reported by the UN-SPIDER script and GISTDA was vastly different. The UN-SPIDER script reported 3,246 affected individuals, while GISTDA reported 47,888. This discrepancy is attributed to the different methods used to determine the number of affected people. In the UN-SPIDER script, the population data was derived from the Global Human Settlement Layer (GHSL) with a spatial resolution of 250 meters, using nighttime light (NTL) data. As shown in Figure 5, NTL data captured by satellites provides valuable insights into human activity and urbanization by measuring the intensity and extent of artificial lights at night. This data can be linked to socioeconomic indicators and development trends [29]. However, the algorithm used to convert NTL data (measured in $W \cdot cm^{-2} \cdot sr^{-1}$) into population counts per pixel is not provided by GHSL, which raises concerns about the accuracy of the population estimates. While urbanization trends can be analyzed using NTL data, the precision of the population numbers remains uncertain.

On the other hand, the population estimate reported by GISTDA also raises questions regarding its data source. It is assumed that GISTDA's figures were based on the total populations of affected sub-districts, which likely resulted in an overestimation of the number of affected people. This is evident in Table 2, where 47,888 affected people are reported, alongside 1,307 affected houses. With these numbers, the average household size is calculated to be 36.6 people per house, which seems implausible. Therefore, the number of affected people and houses reported by GISTDA is questionable. However, more accurate data on affected houses could potentially be obtained through alternative data acquisition methods, such as UAV surveys.

In summary the UN-SPIDER recommended practice is suitable for assessing large areas affected by significant flooding. It is scalable, allowing users to define their own area of interest and time periods. The methodology relies on data from the Copernicus Programme's Sentinel-1 satellite, which means it cannot provide information on floods that occurred before the satellite's launch in July 2014. The strengths of this approach lie in its adaptability to different regions, as it can be easily applied to various locations. Once the area and time period are specified, the process is fully automatic, requiring minimal intervention.

Table 2: The comparison between the UN-SNIPER script and the GISTDA report

Description	UN-SPIDER script	GISTDA
Flood extent area [ha]	36,409	37,425
Affected crop area [ha]	11,107	24,395
No. of affected people	3,246	47,888

Additionally, the workflow is efficient, enabling near-real-time monitoring of flood events globally. The method operates independently of cloud cover, which is essential for consistent flood detection. Moreover, it allows for the integration of auxiliary datasets, such as slope data [30][31]and [32], to help delineate flood extents more accurately. The approach also provides valuable information on the exposed population, affected cropland, and urban areas, enhancing its utility for disaster management and recovery efforts.

However, there are some limitations to consider. False positives may arise from surface changes that are not related to flooding, and detecting floods in urban or densely vegetated areas is particularly challenging. The methodology also cannot capture flood peaks due to the acquisition frequency of Sentinel-1, meaning that the timing of satellite passes may miss the highest points of the flood event. Additionally, differences in the satellite's relative orbits may lead to false positives, and processing large areas can introduce border noise errors. The spatial resolution of datasets like MODIS Land Cover (500 m) and JRC GHSL Population (250 m) may also create some uncertainty when assessing the extent of flood-related damage.

To mitigate the impact of future floods, the flood map can serve as a crucial tool. By identifying flood-prone areas, flood maps enable authorities to assess risk and prioritize flood management efforts in the most vulnerable locations. Real-time data from flood maps, including river levels and rainfall predictions, can support early warning systems, allowing residents and businesses in the market to prepare and respond in advance. The maps can also guide infrastructure planning by highlighting areas where drainage systems need improvement or where flood barriers may be necessary. Moreover, the maps can inform land use planning decisions, helping to ensure that flood-prone areas are not developed and encouraging the creation of green spaces or water retention zones to reduce runoff. Additionally, flood maps can assist in creating evacuation routes and identifying safe zones, which is critical for disaster preparedness and response.

5. Conclusions

The study successfully applied UN-SPIDER's recommended practices to map the 2024 Chiang Rai flood using Sentinel-1 SAR data and Google Earth Engine, demonstrating the effectiveness of satellite-based flood monitoring. The optimal threshold value of 1.25 for change detection aligned closely with ground reports, validating the method's reliability for flood extent mapping. The findings revealed significant inundation in northern Chiang Rai, particularly in Mae Sai district, driven by monsoon rains and inadequate drainage systems. While the approach proved scalable and efficient for large-area assessments, limitations such as spatial resolution constraints in MODIS land cover data and population estimation inaccuracies highlighted areas for improvement. Integrating higher-resolution imagery and ground-based validation could enhance the precision of cropland and urban damage assessments. Despite these challenges, the study underscores the critical role of remote sensing in disaster management, offering timely data for response and recovery efforts. The flood maps generated can inform risk mitigation strategies, including infrastructure planning and early warning systems, to reduce future vulnerabilities. By bridging the gap between space technology and disaster management, this research contributes to building resilience in flood-prone regions like Chiang Rai and provides a replicable framework for global applications. Future work should focus on refining methodologies to address current limitations and expanding the integration of multi-source data for comprehensive flood impact analysis.

References

[1] Thammaboribal, P., Tripathi, N., Nakamura, S. and Lipiloet, S., (2025). Determinations of the Slope of the Chao Phraya Riverbank and Manning's Roughness Coefficient Utilizing Precise Point Positioning (PPP) Measurement Technique. *International Journal of Geoinformatics*, Vol. 21(2), 141–158. https://doi.org/10.52939/ijg.v21i2.3953.

[2] Ginnetti, J. and Milano, L., (2019). Assessing the Impact of Climate Change on Flood Displacement Risk. [Online]. Available: https://api.internal-displacement.org/sites/default/files/publications/documents/201912-climate-change-flood-risk-paper.pdf. [Accessed Feb. 11, 2025].

[3] Vinet, F., (2017). 3-Flood Impacts on Loss of Life and Human Health. *Floods*. Vol. 1, 33-51. https://doi.org/10.1016/B978-1-78548-268-7.50003-1.

[4] Mohammadi, M. Y., Abbasi, E., Farhadian, H. and Asgary, A., (2024). Mitigating the Flood Disaster Effects Through the Implementation of Knowledge Management: A Systematic Literature Review. *Environmental and Sustainability Indicators*. Vol. 23. https://doi.org/10.1016/j.indic.2024.100431.

[5] Wang, L., Cui, S., Li, Y., Huang, H., Manandhar, B., Nitivattananon, V., Fan, X. and Huang, W., (2022). A Review of the Flood Management: from Flood Control to Flood Resilience. *Heliyon*, Vol. 8(11). https://doi.org/10.1016/j.heliyon.2022.e11763.

[6] Tran, T. and Nguyen, D., (2025). Flood Inundation Assessment on Agricultural Land: Integrating High Spatial Resolution Sentinel Data with LiDAR DEM. *International Journal of Geoinformatics*, Vol. 21(3), 71–81. https://doi. org/10.52939/ijg.v21i3.3997.

[7] Khamphilung, P., Konyai, S., Slack, D., Chaibandit, K. and Prasertsri, N., (2023). Flood Event Detection and Assessment using Sentinel-1 SAR-C Time Series and Machine Learning Classifiers Impacted on Agricultural Area, Northeastern, Thailand. *International Journal of Geoinformatics*, Vol. 19(6), 17–29. https://doi.org/10.52939/ijg.v19i6.2691.

[8] Amitrano, D., Di Martino, G., Di Simone, A. and Imperatore, P., (2024). Flood Detection with SAR: A Review of Techniques and Datasets. *Remote Sensing*. Vol. 16(4). https://doi.org/10.3390/rs16040656.

[9] Nguyen, D., M., T., Do, T. N., Nghiem, S. V., Ghimire, J., Dang, K. B., Giang, V. T., Vu, K. C. and Pham, V. M., (2024). Flood Inundation Assessment of UNESCO World Heritage Sites Using Remote Sensing and Spatial Metrics in Hoi An City, Vietnam. *Ecological Informatics*, Vol. 79. https://doi.org/10.1016/j.ecoinf.2023.102427.

[10] United Nations. (N.D.). Step-by-Step: Recommended Practice: Flood Mapping and Damage Assessment Using Sentinel-1 SAR Data in Google Earth Engine. Available: https://www.un-spider.org/advisory-support/recommended-practices/recommended-practice-google-earth-engine-flood-mapping/step-by-step#Step%202:%20Time%20frame%20and%20sensor%20parameters%20selection. [Accessed: Feb. 11, 2024].

[11] Krisanaraj, J., (2025). Flooding in Thailand between August and September 2024 Seen as Historic. [Online]. Available: https://www.nationthailand.com/sustaination/40044461. [Accessed: Feb. 11, 2025].

[12] Thepgumpanat, P. and Setboonsarng, C., (2024). Flooding in Thailand Maroons Thousands in Northern Province. [Online]. Available: https://www.reuters.com/world/asia-pacific/flooding-thailand-maroons-thousands-northern-province-2024-09-12/. [Accessed: Feb. 11, 2025].

[13] Nguyen, D., Chou, T., Hoang, T. and Chen, M., (2023). Flood Susceptibility Mapping Using Machine Learning Algorithms: A Case Study in Huong Khe District, Ha Tinh Province, Vietnam. *International Journal of Geoinformatics*, Vol. 19(7), 1-15. https://doi.org/10.52939/ijg.v19i7.2739.

[14] Djenaliev, A., Kada, M., Chymyrov, A., Hellwich, O., Bairamov, E. and Muraliev, A., (2022). Investigation of Earthquake Deformation Detectability using Sentinel-1 Interferometric Data. *International Journal of Geoinformatics*, Vol. 18(6), 81–96. https://doi.org/10.52939/ijg.v18i6.2453.

[15] Garg, S., Dasgupta, A., Motagh, M., Martinis, S. and Selvakumaran, S., (2024). Unlocking the Full Potential of Sentinel-1 for Flood Detection in Arid Regions. *Remote Sensing of Environment*, Vol. 315. https://doi.org/10.1016/j.rse.2024.114417.

[16] Sadek, M., Li, X., Mostafa, E. and Freeshah, M., (2020). Low-Cost Solutions for Assessment of Flash Flood Impacts Using Sentinel-1/2 Data Fusion and Hydrologic/Hydraulic Modeling: Wadi El-Natrun Region, Egypt. *Advanced in Civil Engineering*, Vol. 2020(1), 1-21. https://doi.org/10.1155/2020/1039309.

[17] Khamnoi, W., Homhuan, S., Suwanprasit, C., and Shahnawaz. (2024). Assessment of Post-Harvest Rice Crop Biomass and Carbon Stock using Remote Sensing Data in Google Earth Engine. *International Journal of Geoinformatics*, Vol. 20(8), 88–101. https://doi.org/10.52939/ijg.v20i8.3459.

[18] Jaelani, L. and Handayani, C., (2022). Spatio-temporal Analysis of Land Surface Temperature Changes in Java Island from Aqua and Terra MODIS Satellite Imageries Using Google Earth Engine. *International Journal of Geoinformatic*s, Vol. 18(5), 1–12. https://doi.org/10.52939/ijg.v18i5.2365.

[19] Boonma, R., Suwanprasit, C. and Homhuan, S., (2024). Modeling Rice Growth and Yield using Integrated Remote Sensing Data on Google Earth Engine. *International Journal of Geoinformatics*, Vol. 20(11), 116–133. https://doi.org/10.52939/ijg.v20i11.3693.

[20] Ouchra, H., Belangour, A. and Erraissi, A., (2023). Comparing Unsupervised Land Use Classification of Landsat 8 OLI Data Using K-means and LVQ Algorithms in Google Earth Engine: A Case Study of Casablanca. *International Journal of Geoinformatics*, Vol. 19(12), 83–92. https://doi.org/10.52939/ijg.v19i12.2981.

[21] Aji, A., Husna, V. and Purnama, S., (2024). Multi-Temporal Data for Land Use Change Analysis Using a Machine Learning Approach (Google Earth Engine). *International Journal of Geoinformatics*, Vol. 20(4), 19–28. https://doi.org/10.52939/ijg.v20i4.3145.

[22] Johary, R., Révillion, C., Catry, T., Alexandre, C., Mouquet, P., Rakotoniaina, S., Pennober, G. and Rakotondraompiana, S., (2023). Detection of Large-Scale Floods Using Google Earth Engine and Google Colab. *Remote Sensing*, Vol. 15(22). https://doi.org/10.3390/rs15225368.

[23] Singh, G. and Rawat, K. S., (2024). Mapping Flooded Areas Utilizing Google Earth Engine and Open SAR Data: A Comprehensive Approach for Disaster Response. *Discovery Geoscience*, Vol. 2(5). https://doi.org/10.1007/s44288-024-00006-4.

[24] Hamidi, E., Peter, B. G., Muñoz, D. F., Moftakhari, H. and Moradkhani, H., (2023). Fast Flood Extent Monitoring with SAR Change Detection Using Google Earth Engine. *IEEE Transactions on Geoscience and Remote Sensing*, Vol. 61, 1-19. https://doi.org/10.1109/TGRS.2023.3240097.

[25] Boonma, R., Suwanprasit, C., Homhuan, S. and Shahnawaz, (2024). Classification of Northern Thai Rice Varieties Using Random Forest (RF) and Support Vector Machine (SVM) on Google Earth Engine with Sentinel Imagery: A Case Study in Buak Khang Subdistrict, San Kamphaeng District, Chiang Mai Province. *International Journal of Geoinformatics*, Vol. 20(9), 27–42. https://doi.org/10.52939/ijg.v20-i9.3539.

[26] Rahman, M. M., Kamruzzaman, M., Deb, L. and Touhidul Islam, H. M., (2025). Flood Mapping, Damage Assessment, and Susceptibility Zonation in Northeastern Bangladesh in 2022 using Geospatial Datasets. *Progress in Disaster Science*, Vol. 25. https://doi.org/10.1016/j.pdisas.2024.100402.

[27] Ting, K. M., (2011). Confusion Matrix. In: Sammut, C., Webb, G.I. (eds) *Encyclopedia of Machine Learning*. Springer, Boston, MA. https://doi.org/10.1007/978-0-387-30164-815-7.

[28] Thammaboribal, P. and Tripathi, N., (2024). Predicting Land Use and Land Cover Changes in Pathumthani, Thailand: A Comprehensive Analysis from 2013 to 2023 Using Landsat Satellite Imagery and CA-ANN Algorithm, with Projections for 2028 and 2038. *International Journal of Geoinformatics*, 20(5), Vol. 1-27. https://doi.org/10.52939/ijg.v20i5.-3225.

[29] Monkhan, N., Phimha, S., Prasit, N. and Senahad, N., (2025). Spatial Distribution Patterns of Colorectal Cancer Patients in Thailand. *International Journal of Geoinformatics*, Vol. 21(2), 159–175. https://doi.org/10.52939/ijg.v21i2.3961.

[30] Ramesh, V. and Sumaira, S., (2020). Urban Flood Susceptibility Zonation Mapping using Evidential Belief Function, Frequency Ratio and Fuzzy Gamma Operator Models in GIS: A Case Study of Greater Mumbai, Maharashtra, India. *Geocarto International*, Vol. 37(2), 581–606. https://doi.org/10.1080/10106049.2020.1730448.

[31] Mohd Rasu, M., Suhandri, H., Khalifa, N., Abdul Rasam, A. and Hamid, A., (2023). Evaluation of Flood Risk Map Development through GIS-Based Multi-Criteria Decision Analysis in Maran District, Pahang - Malaysia. *International Journal of Geoinformatics*, Vol. 19(10), 1–16. https://doi.org/10.52939/ijg.v19i9.2873.

[32] Kumne, W. and Samanta, S., (2023). Geospatial Mapping of Inland Flood Susceptibility Based on Multi-Criteria Analysis-A Case Study in the Final Flow of Busu River Basin, Papua New Guinea. *International Journal of Geoinformatics*, Vol. 19(6), 31–48. https://doi.org/10.52939/ijg.v19i6.2693.